CHEMISTRY OF MATERIALS

pubs.acs.org/cm

Article

Anion Binding as a Strategy for the Synthesis of Porous Salts

Alexandra M. Antonio, Michael R. Dworzak, Kyle J. Korman, Glenn P. A. Yap, and Eric D. Bloch*

Cite This: *Chem. Mater.* 2022, 34, 10823−10831

Read Online

ACCESS | Metrics & More | Article Recommendations | Supporting Information

ABSTRACT: Porous salts have recently emerged as a promising new class of ultratunable permanently microporous solids. These adsorbents, which were first reported as ionic solids based on porous cations and anions, can be isolated from a wide variety of charged, permanently porous coordination cages. A challenge in realizing the full tunability of such systems, however, lies in the fact that the majority of coordination cages for which surface areas have been reported are comprised of charge-balanced inorganic and organic building blocks that result in neutral cages. As such, most reported permanently porous coordination cages cannot be used as reagents in the synthesis of porous salts. Here, we show that the facile reaction of TBAX (TBA^+ = tetra-*n*-butylammonium; X = F^- and Cl^-) with molybdenum paddlewheel-based coordination cages of the M_4L_4 and $M_{24}L_{24}$ lantern and cuboctahedra structure types, respectively, affords charged cages by virtue of coordination of halide anions to the internal and/or external metal sites on these structures, as confirmed by single-crystal X-ray diffraction, X-ray photoelectron spectroscopy, and nuclear magnetic resonance (NMR) spectroscopy. At a practical level, the TBAX/cage reactions, which are fully reversible upon isolation of the cage with the appropriate solvent, solubilize otherwise rigorously insoluble cages. This method significantly increases the solution processability of these highly porous solids. Toward the formation of new porous salts, halide binding also serves to incorporate charge on neutral cages and make them amenable to simple salt metathesis reactions to afford new porous salts based on anions and cations with intrinsic porosity. A combination of diffraction methods and a suite of spectroscopic tools confirms speciation of the isolated solids, which represent a new class of highly tunable porous salts. Ultimately, this work represents a roadmap for the preparation of new porous solids and showcases the utility and broad applicability of anion binding as a strategy for the synthesis of porous salts.

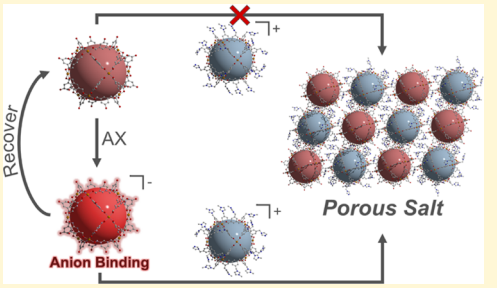

INTRODUCTION

Among permanently porous molecular materials, porous coordination cages (PCCs, or metal−organic polyhedra (MOPs)) have received renewed attention over the past few years as reports of porous structures have increased and their utility for gas storage,[1,2] gas separation,[3] catalysis,[4,5] as membrane additives,[6] and in biomedical applications has been firmly established.[7] As compared to extended network solids, such as metal−organic frameworks (MOFs),[8] porous aromatic frameworks (PAFs),[9] and covalent-organic frameworks (COFs),[10] permanently porous molecules have the distinct advantage in that their discrete nature allows for solution processability, which can be leveraged in the synthesis,[11] purification,[12] modification,[13] and utilization of these porous solids. A challenge here, however, is that many permanently porous coordination cages display minimal solubility in common organic solvents.[14,15] As such, they exhibit bulk properties that are analogous to those of MOFs, PAFs, and COFs, rather than molecular species.

Analogous to modification strategies used in porous organic cage (POCs) syntheses,[16] porous coordination cages can be functionalized with targeted organic groups to tune their solubility,[13] stability,[15] and porosity.[17] These routes can be employed prior to cage formation, in the straightforward synthesis of functionalized ligands,[18] or after cage synthesis.[13,19] This latter strategy, which is similar to post-synthetic modification of MOFs,[20] has the distinct advantage in that solubility of functionalized cages facilitates modification and characterization. However, modification strategies can become complex as the surface area, stability, and solubility of coordination cages are typically related and modification of a structure to increase solubility often leads to decreases in the surface area.[21]

Recently, a number of reversible strategies for solubilizing permanently porous coordination cages have been reported, primarily utilizing rhodium-based $M_{24}L_{24}$ cuboctahedral coordination cages.[22,23] Both the ligands and the paddlewheel-based coordinatively unsaturated metal cations that comprise these highly tunable structures serve as a site for reversible post-synthetic modification via covalent and coordination chemistry approaches. In a straightforward

Received: May 16, 2022
Revised: October 25, 2022
Published: December 15, 2022

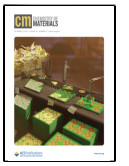

route, pH tuning or cation exchange reactions were utilized to transfer cage and metal-coordinated cargo between immiscible solvents.[24] It was subsequently shown that a long alkyl chain-containing coordination solubilizer could be used to solubilize otherwise insoluble $Rh_{24}(bdc)_{24}$ by coordination to the exterior rhodium sites on the material.[25] Given the general Lewis acidity of cations in paddlewheel-based permanently porous coordination cages, we reasoned that reversible anion binding could be utilized to tune the solubility and thus solution processability of these materials in a reversible manner. Importantly, this approach is highly tunable as the counter cation for a given anion can be selected based on target solvent. Further, it is broadly applicable for cages without inherent charge. It is notable that ion binding has been extensively studied in coordination cages, where the encapsulation of anions by receptors in aqueous or organic media have broad applications in biological, environmental, and industrial areas.[26] Many cationic coordination cages have been shown to bind anions in polar organic solvents where selectivity and solubility can be tuned through straightforward functionalization routes.[27−31] It is expected that translation of this approach to permanently porous coordination cages functionalized with different ligands, those that retain porosity in the solid state upon solvent evacuation, will lend a new level of tunability to these promising materials.

The incorporation of charged units into or onto otherwise neutral porous coordination cages also serves as a unique approach in preparing new classes of porous salts. These materials that typically consist of pairs of oppositely charged, permanently porous, coordination cages were recently reported by us[32] and followed up on by a number of additional researchers.[33−36] A particular challenge in the preparation of novel porous salts, however, is the fact that the vast majority of permanently microporous coordination cages are in fact charge-neutral in their native state. Although ligand functionalization, metal oxidation state tuning, and metal coordination sphere tuning may be employed to achieve charged porous cages, these strategies can interfere with cage formation and afford nonporous phases. In the work reported here, we detail the use of reversible anion binding to the exterior and/or interior metal cation sites in paddlewheel-based coordination cages to impart solubility for a class of highly porous, but insoluble cages and as a means to incorporate charge in neutral cages for the isolation of porous salts.

EXPERIMENTAL SECTION

Materials and Methods. With the exception of solvents, all reagents were obtained from commercial vendors and used without purification. Dimethylformamide and methanol were obtained from a solvent drying system and stored in N_2 atmosphere gloveboxes over 4 and 3 Å sieves, respectively. Commercial anhydrous TBAF in THF was freeze−pump−thawed before storing in a N_2 atmosphere glovebox over 3 Å sieves. Commercial anhydrous TBACl was dried under dynamic vacuum for 12 h on a Schlenk line to remove residual water. Detailed ligand syntheses are presented in the Supporting Information.

Thermogravimetric analyses (TGA) were carried out from 30 to 600 °C at a 2 °C/min heating rate with a TA Q5000 TGA under a nitrogen flow. Low-pressure CO_2 and N_2 adsorption measurements were obtained on a Micromeritics Tristar 3000 at 195 K and a Micromeritics Tristar II Plus at 77 K, respectively. ^{1}H NMR and ^{19}F NMR spectra were recorded on a Bruker AV 400 MHz spectrometer and the obtained data were manipulated in a MestReNova NMR processor software. Infrared (IR) spectra were carried out with a Bruker α II instrument affixed with a diffuse reflectance ATR attachment. Ultraviolet−visible (UV−vis) experiments were carried out with an AvaSpec-ULS2048CL with a deuterium−halogen light. Elemental analyses were performed on Thermo Fisher Kα X-ray photoelectron spectroscopy (XPS) at the University of Delaware's Surface Analysis Facility. Powder X-ray diffraction patterns were recorded with Bruker D8 X-ray powder diffractometer with a Cu Kα radiation (1.54 nm) housed in the Advanced Materials Characterization Laboratory at the University of Delaware. Scanning electron microscopy images and energy-dispersive X-ray spectra were taken using an SEM/FIB Auriga 60 also housed in the Advanced Materials Characterization Laboratory.

^{1}H NMR Digestion Measurements. Acid digestions were performed by adding two drops of 35 wt % deuterium chloride and DMSO-d_6 to a 4 mL vial containing ∼5 mg of the material.

^{1}H NMR Cage Solubilization via Salt Addition. To solubilize a given cage, 0.5−2 equiv of TBAX (X = F, Cl, or Br) salt was added based on the formula unit of each cage. For example, a 2 equiv salt addition to an $M_{24}L_{24}$ cage is actually 48 equiv per whole cage. Similarly, a 2 equiv salt addition to an M_4L_4 cage represents 8 equiv per cage.

Scanning Electron Microscopy−Energy-Dispersive X-ray Spectroscopy (SEM−EDS). To prepare the samples, the dried material was placed on a double-sided carbon tape that was attached to an aluminum pin. The samples were sputtered using a Pd/Au alloy for 60 s while rotating at a 45° angle. The samples were then imaged using a 3 kV accelerating voltage via the SEM/FIB Auriga 60. For elemental analysis via EDS, an accelerating voltage of 10 kV was used.

X-ray Photoelectron Spectroscopy (XPS) Analysis. To prepare air-sensitive samples for analysis, an air-tight sample holder was pumped into a N_2 glovebox after applying carbon tape to the grid. The dried materials were adhered to the carbon tape in the glovebox and the sample holder was sealed under N_2. The sample holder was then evacuated in the glovebox chamber for 30 min so it could be loaded into the XPS chamber under vacuum. A Fisher Kα spectrometer equipped with monochromatic Al Kα X-rays (1486.7 eV) was used to analyze the samples where the operating pressure in the main chamber was less than 1×10^{-8} Torr. The X-ray spot size on Kα was elliptical in shape with a semimajor axis of roughly 400 μm.

Synthesis of $Mo_4(hdp)_4$ Crystals. $Mo_2(OAc)_4$ (0.023 g, 0.05 mmol) and 6,6′-(5-hydroxy-1,3-phenylene)dipicolinic acid (0.0167 g, 0.05 mmol) were added to a 4 mL scintillation vial and dissolved in 2.4 mL of DMF and 0.6 mL of MeOH. Upon heating at 85 °C in a N_2 glovebox for 1 day, crystals formed. The mother liquor was decanted and the isolated crystals were washed with anhydrous methanol 3 times, exchanging the solvent every 8 h, and dried under vacuum to yield an orange powder.

Synthesis of Bulk $Mo_4(hdp)_4$ Powder. $Mo_2(OAc)_4$ (0.092 g, 0.2 mmol) and 6,6′-(5-hydroxy-1,3-phenylene)dipicolinic acid (0.0668 g, 0.2 mmol) were added to a 20 mL scintillation vial and dissolved in 6 mL of DMF and 6 mL of MeOH. Upon heating at 85 °C in a N_2 glovebox for 2 days, the crystalline material formed. The mother liquor was decanted and the solid washed with anhydrous methanol 3 times, exchanging the solvent every 8 h, and dried under vacuum to yield 0.0536 g of an orange powder (62.3% yield).

Synthesis of $H[Mo_4(hdp)_4F]$ Crystals. $Mo_4(hdp)_4$ (0.0036 g, 0.002 mmol) and 1 M TBAF in THF (0.015 g, 0.016 mmol, 8 equiv per cage) were added to a 4 mL scintillation vial and dissolved in 1.8 mL of DMSO upon heating at 85 °C in a N_2 glovebox. Once the cage was dissolved, 1.2 mL of MeOH was layered onto the solution. The crystals formed after 1 day.

Synthesis of $Mo_4(tdp)_4$ Crystals. $Mo_2(OAc)_4$ (0.023 g, 0.05 mmol) and 6,6′-(5-methyl-1,3-phenylene)dipicolinic acid (0.0167 g, 0.05 mmol) were added to a 4 mL scintillation vial and dissolved in 3 mL of *N*,*N*-dimethylpropyleneurea (DMPU) with four drops of pyridine. Upon heating at 85 °C in a N_2 glovebox for 2 days, the crystals formed. The mother liquor was decanted and the crystals washed with anhydrous methanol 3 times, exchanging the solvent every 8 h, and dried under vacuum to yield an orange powder.

Synthesis of Bulk $Mo_4(tdp)_4$ Powder. $Mo_2(OAc)_4$ (0.092 g, 0.2 mmol) and 6,6′-(5-methyl-1,3-phenylene)dipicolinic acid (0.0668 g,

https://doi.org/10.1021/acs.chemmater.2c01476
Chem. Mater. 2022, 34, 10823−10831

0.2 mmol) were added to a 20 mL scintillation vial and dissolved in 6 mL of DMF and 6 mL of MeOH. Upon heating at 85 °C in a N_2 glovebox for 2 days, the crystalline material formed. The mother liquor was decanted and the solid washed with anhydrous methanol 3 times, exchanging the solvent every 8 h, and dried under vacuum to yield 0.0610 g of an orange powder (71.2% yield).

Synthesis of TBA[Mo_4(tdp)$_4$F] Crystals. Mo_4(tdp)$_4$ (0.0036 g, 0. 002 mmol) and 1 M TBAF in THF (0.015 g, 0.016 mmol, 8 equiv per cage) were added to a 4 mL scintillation vial and dissolved in 1.5 mL of DMF upon heating at 85 °C in a N_2 glovebox. Once the cage was dissolved, 1.5 mL of THF was added to the vial. Upon heating at 85 °C in a N_2 glovebox for 2 days, the crystals formed.

Synthesis of Mo_4(adp)$_4$ Crystals. $Mo_2(OAc)_4$ (0.023 g, 0.05 mmol) and 6,6′-(5-methoxy-1,3-phenylene)dipicolinic acid (0.0175 g, 0.05 mmol) were added to a 4 mL scintillation vial and dissolved in 1.5 mL of DMF and 1.5 mL of MeOH. Upon heating at 85 °C in a N_2 glovebox for 2 days, the crystals formed. The mother liquor was decanted and the solid washed with anhydrous methanol 3 times, exchanging the solvent every 8 h, and dried under vacuum to yield an orange powder. Bulk material was isolated in an analogous manner at 4× scale in 20 mL scintillation vials. The scaled-up material was similarly isolated and washed and afforded 0.0445 g of an orange powder (50.1% yield).

Synthesis of TBA[Mo_4(adp)$_4$F] Crystals. Mo_4(adp)$_4$ (0.0037 g, 0. 002 mmol) and 1 M TBAF in THF (0.015 g, 0.016 mmol, 8 equiv per cage) were added to a 4 mL scintillation vial and dissolved in 1.2 mL of DMF upon heating at 85 °C in a N_2 glovebox. Once the cage was dissolved, 1.8 mL of THF was added to the vial. Upon heating at 85 °C in a N_2 glovebox for 2 days, the crystals formed.

Synthesis of [Mo_{24}(MImid-bdc)$_{24}$]Br_{24}. $Mo_2(OAc)_4$ (0.092 g, 0.2 mmol) and 5-methyl-imidazoliumisophthalic acid bromide salt (0.068 g, 0.2 mmol) were added to a 20 mL scintillation vial and dissolved in 10 mL of a ratio of 40:60 DMF/MeOH. After heating at 85 °C in a dry bath for 2 days, when no crystalline material formed, 10 mL of diethyl ether was used to precipitate the bulk material. The powder was washed with anhydrous diethyl ether 3 times, exchanging the solvent every 8 h, and dried under vacuum to yield 0.0885 g of an orange powder (85.6% yield). For the purposes of charge balance and molecular weight calculations, the assumed counter ion was bromide.

Synthesis of Mo_{24}(^{t}Bu-bdc)$_{24}$. The synthesis was reproduced from previously reported methods.[2]

Synthesis of Mo_{24}(OH-bdc)$_{24}$. The synthesis was reproduced from previously reported methods.[13]

Synthesis of Mo_{24}(Me-phenyloxy-bdc)$_{24}$. The synthesis was reproduced from previously reported methods.[37]

Single-Crystal Synthesis of [Mo_{24}(5-OH-bdc)$_{24}$][Mo_{24}(5-MImid-bdc)$_{24}$]Cl_{24}. Mo_{24}(OH-bdc)$_{24}$ (0.0138 g, 0.002 mmol, 1 equiv) was added to a 20 mL scintillation vial and dissolved in 8 mL of DMF upon addition of TBACl (0.0278 g, 0.1 mmol, 50 equiv per cage). In a separate 20 mL scintillation vial, [Mo_{24}(MImid-bdc)$_{24}$]Br_{24} (0.0218 g, 0.002 mmol, 1 equiv) was dissolved in 5 mL of MeOH and 5 mL of DMF. After combining the two solutions in a 20 mL vial and upon heating at 85 °C in a N_2 glovebox for 1 day, the crystals formed. The mother liquor was decanted and the crystals were washed with anhydrous methanol 3 times, exchanging the solvent every 8 h, and dried under vacuum to yield 0.0204 g of an orange, insoluble powder (51.5% yield) based on the formula unit of a 1:1 ratio of Mo_{24}(OH-bdc)$_{24}$/Mo_{24}(MIm-bdc)$_{24}$ of bulk material determined via ^{1}H NMR and single-crystal X-ray analysis.

Single-Crystal Synthesis of [Mo_4(hdp)$_4$]$_4$[Mo_{24}(5-MImid-bdc)$_{24}$]F_{24}. Mo_4(hdp)$_4$ (0.0041 g, 0.0024 mmol, 6 equiv) was added to a 4 mL scintillation vial and dissolved upon heating at 85 °C in 1.5 mL of DMSO upon addition of 1 M TBAF in THF (0.009 g, 0.01 mmol, 4 equiv per cage). In a separate 4 mL scintillation vial, [Mo_{24}(MImid-bdc)$_{24}$]Br_{24} (0.005 g, 0.0004 mmol, 1 equiv) was dissolved in 1.5 mL of MeOH. After combining the two solutions in a 4 mL vial and upon heating at 85 °C in a N_2 glovebox for 1 day, the crystals formed. The mother liquor was decanted and the crystals were washed with anhydrous methanol 3 times, exchanging the solvent every 8 h, and dried under vacuum to yield an orange, insoluble powder. To synthesize bulk material, the synthesis was scaled-up at 4× scale in 20 mL scintillation vials. The isolated solid was similarly washed and then dried under vacuum to yield 0.01636 g of an orange powder (86.2% yield) based on the formula unit of a ∼4:1 ratio of Mo_4(hdp)$_4$/Mo_{24}(MIm-bdc)$_{24}$ of bulk material determined via ^{1}H NMR.

Single-Crystal X-ray Diffraction. X-ray structural analysis for Mo_4(tdp)$_4$, Mo_4(adp)$_4$, TBA[Mo_4(tdp)$_4$F], TBA[Mo_4(adp)$_4$F], Mo_4(hdp)$_4$, [Mo_4(hdp)$_4$F]$_4$[Mo_{24}(5-MImid-bdc)$_{24}$], Mo_4(hdp)$_4$F, Mo_{24}(5-OH-bdc)$_{24}$, and [Mo_{24}(5-OH-bdc)$_{24}$][Mo_{24}(5-MImid-bdc)$_{24}$]: Crystals were mounted using viscous oil onto a plastic mesh and cooled to the data collection temperature. Data were collected on a D8 Venture Photon III diffractometer with Cu Kα radiation (λ = 1.54178 Å) focused with Goebel mirrors. Unit-cell parameters were obtained from fast scan data frames, 1°/s ω, of an Ewald hemisphere. The unit-cell dimensions, equivalent reflections, and systematic absence in the diffraction data are consistent with *Cc* and *C2/c* for TBA[Mo_4(tdp)$_4$F]; *I*4, *I*-4, and *I*4/*m* for [Mo_4(hdp)$_4$F]$_2$[Mo_{24}(5-MImid-bdc)$_{24}$] and Mo_{24}(5-OH-bdc)$_{24}$; uniquely, *P*2$_1$/*n* for Mo_4(hdp)$_4$F; and, uniquely, *P*2$_1$/*c* for [Mo_{24}(5-OH-bdc)$_{24}$][Mo_{24}(5-MImid-bdc)$_{24}$]. No symmetry higher than triclinic was observed in Mo_4(tdp)$_4$, Mo_4(adp)$_4$, TBA[Mo_4(adp)$_4$F], and Mo_4(hdp)$_4$. Refinement in the centrosymmetric space group option for the nonunique cases yielded chemically reasonable and computationally stable results of refinement. The data were treated with multiscan absorption corrections.[38] Structures were solved using intrinsic phasing methods[39] and refined with full-matrix, least-squares procedures on *F*.[39,40]

Each polyhedral structure is located at an inversion center. For [Mo_4(hdp)$_4$F]$_2$[Mo_{24}(5-MImid-bdc)$_{24}$] and Mo_{24}(5-OH-bdc)$_{24}$, the compound molecule is located at the intersection of a mirror plane perpendicular to a four-fold axis. The disordered cell contents of highly porous metal−organic polyhedral (MOP) complexes result in diffraction data that are limited in coverage and resolution. As a result, it is common to have multiple restraints and constraints, incompletely assigned moieties, and high residuals in the structural model. Presumably disordered solvent molecules and nonlocatable parts of moieties in Mo_4(tdp)$_4$, Mo_4(hdp)$_4$, [Mo_4(hdp)$_4$F]$_2$[Mo_{24}(5-MImid-bdc)$_{24}$], Mo_4(hdp)$_4$F, Mo_{24}(5-OH-bdc)$_{24}$, and [Mo_{24}(5-OH-bdc)$_{24}$]-[Mo_{24}(5-MImid-bdc)$_{24}$] were treated as diffused contributions with identities assigned to be chemically reasonable based on the synthesis, ionic charge balances, and electron counts from the Squeeze results.[41] The DMSO solvent and the central oxygen atom in Mo_4(tdp)$_4$ were located disordered in two positions with refined site occupancies of 89/11 and 68/32, respectively. Two DMF solvent molecules in Mo_4(adp)$_4$ were found disordered in two positions with refined site occupancies of 54/46 and 64/36, respectively. A central atom peak in Mo_4(adp)$_4$ appears to be a partially occupied oxygen atom, assigned as water, whose occupancy is apparently tied to one of the disordered DMF molecules located near the center. The NBu_4^+ cation, THF solvent molecule, and one of two DMF solvent molecules are each located at a two-fold in TBA[Mo_4(tdp)$_4$F] with the cation and THF molecule also disordered with respect to each other by the two-fold symmetry. In TBA[Mo_4(adp)$_4$F], the cation and a DMF solvent molecule are similarly disordered in two positions with a 65/35 refined site distribution with a net half-occupancy since they are also disordered with respect to each other by an inversion center.

Nonhydrogen atoms were refined with anisotropic displacement parameters except in [Mo_4(hdp)$_4$F]$_2$[Mo_{24}(5-MImid-bdc)$_{24}$] where only the metal atoms and fluorine atoms could be refined anisotropically. H-atoms in [Mo_4(hdp)$_4$F]$_2$[Mo_{24}(5-MImid-bdc)$_{24}$] were ignored except in the formula. It is unclear whether the oxygen central atom in Mo_4(tdp)$_4$ is a water molecule and H-atoms can neither be located nor assigned. The H-atoms for the presumed central water molecule in Mo_4(adp)$_4$ were initially located from the diff map but were refined with idealized geometry. All other hydrogen atoms were treated as idealized contributions with geometrically calculated positions and with U_{iso} equal to 1.2 U_{eq} (1.5 U_{eq} for methyl) of the attached atom.

https://doi.org/10.1021/acs.chemmater.2c01476
Chem. Mater. 2022, 34, 10823−10831

Atomic scattering factors are contained in the SHELXTL program library.[39] The structures have been deposited at the Cambridge Structural Database under the following CCDC depositary numbers: CCDC 2089305, 2089308−10, 2143096-8, 2110116, and 2143099.

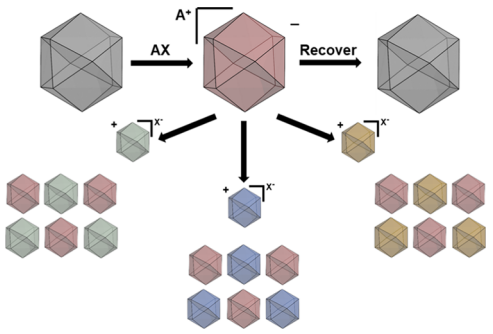

Figure 1. Generalized scheme for the solubilization of cages using salts (red polyhedron) and their subsequent recovery via methanol precipitation (gray polyhedron) or combination with a cationic PCC of different architecture (green, blue, and orange polyhedra) to form porous salts.

RESULTS AND DISCUSSION

As a starting point for this approach, we targeted the solubilization of lantern-type M_4L_4 paddlewheel cages (Figure 2, top) as we have found that the interior of these cages, with

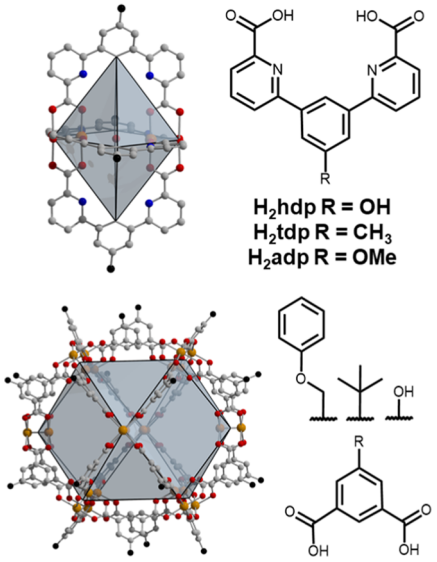

Figure 2. (Top) Functionalized benzene dipicolinic acid ligands and resulting M_4L_4 lantern-type cages used in the synthesis of porous salts. (Bottom) Functionalized isophthalic acid ligand and resulting $M_{24}L_{24}$ cuboctahedral-type cages used here.

M−M distances of approximately 4.5−5 Å, are uniquely suited for the binding of anions. Indeed, the importance of this binding site has been predicted for related lantern-type cages,[42] and we have found that crystal structures of these types of materials typically feature M−O−M units on their interior where the oxygen atom from a solvent molecule (H_2O, MeOH, DMF) is bound between the interior metals (Figures S56 and S58). Our previous work in this area has focused on pyridine- or benzene-based ligands H_2pdb (pyridine dibenzoic acid) and H_2tdb (toluene dibenzoic acid), respectively.[43] Although crystal structures of $M_4(pdb)_4$ and $M_4(tdb)_4$ cages feature metal-bound solvent molecules on their interior surfaces, we were unable to solubilize these materials by halide binding via reaction with TBAX (TBA = tetra-*n*-butylammonium; X = F^-, Cl^-, Br^-) regardless of the identity of the cation. This is not entirely unsurprising given the proximity of the C−H groups on the ligand to the M−M unit inside the cage.

To facilitate anion binding in the interior of the cages, picolinic acid-based ligands were prepared. These ligands (Figure 2) feature two nitrogen atoms on the ligands and a single C−H group per ligand on the interior surfaces of the resulting cages. Straightforward coupling reactions afford hydroxy, toluene, and anisole-benzene-based bispicolinic acid ligands (H_2hdp, H_2tdp, and H_2adp, respectively). Given the propensity of $Mo_2(OAc)_4$ to afford paddlewheel-based cages, the reaction of this salt with picolinic acid ligands in DMF or DMSO affords a highly crystalline cage in nearly quantitative yield. Single-crystal X-ray diffraction experiments reveal that the cages adopt the expected M_4L_4 lantern configuration. Similar to what was observed for previously reported $M_4(pdb)_4$ cages, the ligands in these structures are significantly distorted out of planarity although they have fewer C−H interactions on their interior surface. The paddlewheel units in the three structures feature interior M−M distances of 5.06−5.21 Å. As the interior is an optimal solvent binding pocket, all three structures contain M-solv-M moieties where solv = H_2O, DMF, or MeOH. As expected, the oxygen atom of the solvent molecule is approximately halfway between molybdenum cations. Given the nature of these cages, they display only a moderate CO_2-accessible surface area upon solvent exchange and activation with BET (Langmuir) surface areas ranging from 109 to 137 (165−295) m^2/g.

Although the three novel cages reported here are insoluble in most organic solvents and only display limited solubility in highly polar solvents such as DMF or DMSO, it is expected that incorporation of anionic species between molybdenum paddlewheels, and the associated cations used in this process, can be used to increase solubility and solution processability. For all three cages, stirring cage crystals in DMF or DMSO in the presence of TBAF at elevated temperatures completely solubilized the cage in as little as 1 h (Figures S106−S108). $Mo_4(hdp)_4$ is soluble in DMSO, $Mo_4(adp)_4$ in DMF, and $Mo_4(tdp)_4$ in DMF and DMSO during this treatment, while nonpicolinic acid derivatives ($Mo_4(tdb)_4$ and $Mo_4(pdb)_4$) are completely insoluble. Utilization of a larger halide significantly limits the utility of this approach with $Mo_4(tdp)_4$ displaying only slight DMF solubility, while the remaining cages are insoluble upon treatment with TBACl. We were completely unsuccessful in solubilizing cages with Br^- salts regardless of the solvent choice. These later observations are not entirely unexpected given the limited size of the interior of the cage. Reported halide-bridged (M_2−X−M_2) paddlewheels typically feature M−M (paddlewheel−paddlewheel) distances of ∼4.4−5.2 Å across the halide,[44] which would be expected to be compatible with the paddlewheels in lantern-type cages. However, the M−X−M angles in these structures are significantly nonlinear (Table S3). $K[Mo_2(OAc)_4Cl]$, for example, is a polymeric structure based on chloride-bridged paddlewheel units with 5.158 Å separation. The Mo−Cl−Mo angle in this molecular species is significantly bent at 128.4°.

https://doi.org/10.1021/acs.chemmater.2c01476
Chem. Mater. 2022, 34, 10823−10831

This necessary angle between paddlewheel units for halides larger than fluoride is incompatible with the structure of lantern-type cages.

Single-crystal X-ray diffraction experiments for two of the three isolated cages confirm a single fluoride is coordinated to the interior position between molybdenum cations (Figure 3).

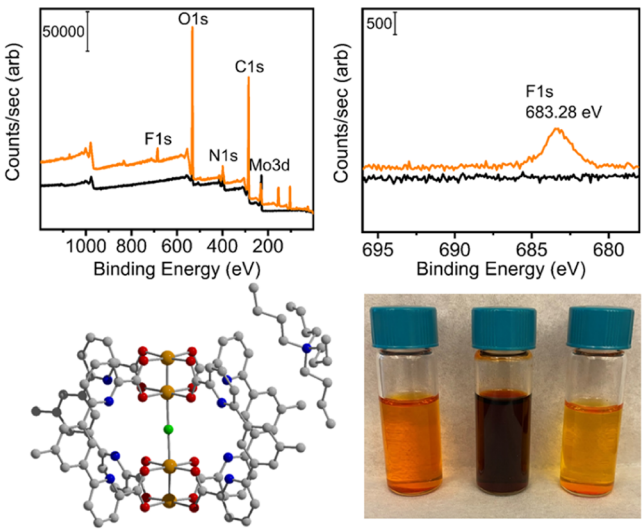

Figure 3. (Top left and right) XPS survey and high-resolution fluorine spectra for $Mo_4(tdp)_4$ (black) and TBA[$Mo_4(tdp)_4F$] (orange), confirming the presence of metal-bound fluoride. (Bottom left) Single-crystal structure of TBA[$Mo_4(tdp)_4F$] where the interior cavity of the cage features molybdenum-bound F^- with a Mo−Mo distance of 4.576 Å and Mo−F distances of 2.288 Å. Orange, red, blue, green, and gray spheres represent molybdenum, oxygen, nitrogen, fluorine, and carbon atoms, respectively. Hydrogen atoms and solvent molecules have been omitted. (Bottom right) TBAF treatment (center vial) significantly increases the solubility of the cage as compared to no treatment (left vial) and after isolation and methanol exchanges (right vial).

The fluoride anion lies at a crystallographic inversion center resulting in a linear (180.0°) Mo_2−F−Mo_2 adduct for both TBA[$Mo_4(tdp)_4F$] and TBA[$Mo_4(adp)_4F$]. In both cages, the paddlewheel−paddlewheel distance is significantly decreased from ∼5.2 to ∼4.6 Å upon fluoride binding, while the Mo−Mo distance within a paddlewheel is essentially unchanged upon fluoride binding with an average of 2.116(5) Å for both neutral and fluoride-containing cages (Table S2). The charge-balancing TBA cations are located at a face of the cage near the Mo_2−F−Mo_2 unit and, in both materials, essentially form one-dimensional (1-D) channels of cations between stacked columns of cages (Figures S57 and S59). ^{1}H NMR spectra of dissolved crystals are consistent with crystallographic characterization and confirm the expected 1:1 cage:cation ratio (Figures S21 and S23), which was further confirmed by ion chromatography for a digested sample. We were unable to observe fluorine resonances in ^{19}F spectra, likely a result of position of the cation between the slightly paramagnetic paddlewheel units. However, the presence of fluoride in bulk material was confirmed by XPS analysis, which displays signals consistent with M−F moieties (Figures S86 and S87). Although we were unable to obtain diffraction-quality single crystals of TBA[$Mo_4(hdp)_4F$], NMR, XPS, IR, and UV−vis experiments confirm the existence of these species upon solubilization (see the Supporting Information for full characterization details). We observe additional resonances in ^{19}F spectra upon addition of excess equivalents of TBAF, including HF_2^- and species that are likely bound on the exterior metal cations of the cages, which are typically otherwise occupied by solvent molecules.

Importantly, solubilized cages can be isolated by simple precipitation protocols. Addition of methanol to DMF or DMSO solutions of fluoride-containing cages affords the product in quantitative yield. Upon solvent exchange and mild activation, the cages become insoluble and display surface areas and powder X-ray diffraction patterns that are similar to those of the starting cages (Figures 3 and S101, S64−S66 and Table S5). XPS analysis of activated cages indicates $Mo_4(adp)_4$ and $Mo_4(tdp)_4$ still contain metal-bound fluoride after solvent exchange and desolvation. Acid-promoted decomposition and digestion of these cages reveals that although they contain fluoride, there is no longer TBA^+ present as the counter cation and suggests bound HF, a common impurity in organic fluoride sources. Indeed, ^{19}F NMR spectra consistently indicate the presence of HF_2^-, which is commonly present in TBAF, a result of the reactivity of F^- and the documented difficulty in obtaining anhydrous fluoride salts.[45] Gas adsorption analyses are consistent with this interpretation as surface areas are actually slightly increased after fluoride treatment and isolation as the encapsulated HF has a lower molar mass and volume than methanol, DMF, or DMSO that is typically present inside these cages and not removed during the mild activation protocols we employ. Although the putatively Mo_2−HF−Mo_2-containing cages are poorly soluble in common organic solvents, they can be redissolved by simply exposing them to additional TBAF to give a soluble cage via the following reaction: Mo_2−HF−Mo_2 + 2TBAF → TBA-(HF_2) + TBA(Mo_2−F−Mo_2). We are currently working on expanding this approach to a variety of noncoordinating bases where deprotonation of encapsulated HF can afford solubilized cages.

As the porosity of these small M_4L_4 lantern cages is somewhat limited, we next turned to solubilizing paddlewheel-based cages of larger $M_{24}L_{24}$ cuboctahedral structure types as they have reported N_2-accessible surface areas orders of magnitude higher.[21] A particular challenge in working with these materials, however, is the highest surface area cuboctahedral cages typically display limited solubility, thus making them promising candidates for anion binding as a means to impart solubility. Three specific molybdenum-based materials, Mo_{24}(5-Me-phenyloxy-bdc)$_{24}$, Mo_{24}(5-^{t}Bu-bdc)$_{24}$, and Mo_{24}(5-OH-bdc)$_{24}$, were investigated in this regard as they have N_2-accessible surface areas ranging from 660 to 1300 m^2/g and low solubility in most solvents.[46] The reaction of these cages with TBAX salts was expected to produce soluble, charged species that could either be recovered as neutral, porous solids or incorporated into porous salts where both the cationic and anionic components are porous cages. As the halides incorporated into these structures could coordinate to metal cation sites on the interior and exterior surfaces of the cage, we were not restricted to the use of TBAF for solubilization. Indeed, the reaction of Mo_{24}(5-OH-bdc)$_{24}$ with a two-fold excess of TBACl in DMF afforded a highly soluble species upon mild heating. Although we were unable to obtain diffraction-quality single crystals of TBA$_x$[Mo_{24}(5-OH-bdc)$_{24}Cl_x$], NMR and UV−vis experiments confirm the existence of this species upon solubilization (Figures S35 and S68).[46] Importantly, and analogous to the reversibility in

https://doi.org/10.1021/acs.chemmater.2c01476
Chem. Mater. 2022, 34, 10823−10831

TBAF binding in M_4L_4 cages, pure Mo_{24}(5-OH-bdc)$_{24}$ can be isolated via precipitation or crystallization from DMF with methanol as the antisolvent, as verified by ^{1}H NMR, XPS, and IR spectroscopy (Figures S36, S75, and S88). Analysis of single crystals of the isolated sample reveals the isolated material adopts the same unit cell, space group, and structure as the as-synthesized starting material. Utilization of less polar solvents to precipitate the solid from TBA$_x$[Mo_{24}(5-OH-bdc)$_{24}$Cl$_x$]-containing solutions affords a cage with varying levels of TBACl. Precipitation of the solid with THF, benzene, or diethyl ether affords TBA$_{13}$[Mo_{24}(5-OH-bdc)$_{24}$Cl$_{13}$] as confirmed by ^{1}H NMR and XPS spectra (Figures 4 and S37–S39).

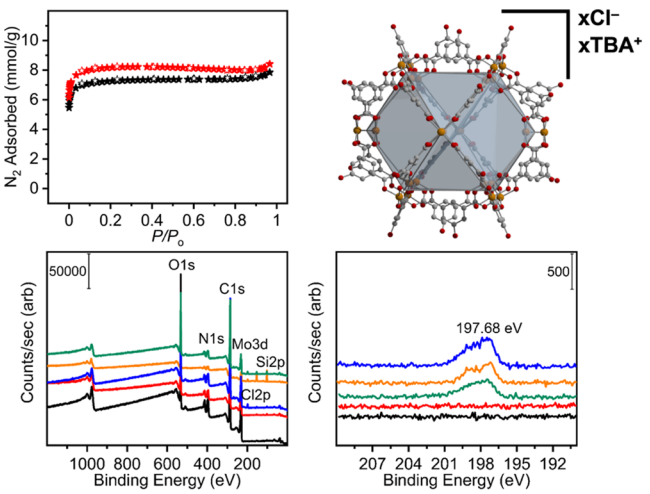

Figure 4. (Top left) N_2 adsorption in Mo_{24}(5-OH-bdc)$_{24}$ at 77 K for samples that were washed with THF (black) or treated with TBACl and subsequently recovered from MeOH (red) corresponding to BET (Langmuir) surface areas of 647 (726) and 726 (806) m^2/g. Closed and open symbols denote adsorption and desorption. (Top right) Single-crystal structure of Mo_{24}(5-OH-bdc)$_{24}$. Orange, red, and gray spheres represent molybdenum, oxygen, and carbon atoms, respectively. Hydrogen atoms and solvent molecules have been omitted. (Bottom left and right) XPS survey spectra and high-resolution chloride spectra for as-synthesized Mo_{24}(5-OH-bdc)$_{24}$ (black) vs Mo_{24}(5-OH-bdc)$_{24}$ recovered from TBACl treatment with methanol (red), THF (green), Et_2O (orange), or benzene (blue).

The broad applicability of this approach was confirmed by targeting $Mo_{24}L_{24}$ cages that have previously been shown to be completely insoluble in all common organic solvents. Here, TBAX salts can be used to solubilize Mo_{24}(5-^{t}Bu-bdc)$_{24}$ and Mo_{24}(5-Me-phenyloxy-bdc)$_{24}$. Given the high thermal stability and directional arene–arene interactions in Mo_{24}(5-Me-phenyloxy-bdc)$_{24}$ in the solid state,[37] TBAF is required to solubilize the material, while Mo_{24}(5-^{t}Bu-bdc)$_{24}$ can be dissolved upon reaction with either TBACl or TBAF. The smaller, more strongly coordinating F^- anion is required to solubilize the aryl-functionalized congener. Although we were unable to obtain diffraction-quality single crystals of halide-containing cages, likely a result of the disorder of TBA cations in the structures, both the external and internal metal cations in the materials are accessible for anion binding. Similar to TBACl-solubilized Mo_{24}(OH-bdc)$_{24}$, NMR, XPS, IR, and UV–vis experiments confirm the persistence of all three cages upon solubilization (see the Supporting Information for full characterization details). Here too, isolation via precipitation with coordinating polar solvents affords pure starting cage with no detectable levels of the TBACl salt. Utilization of TBAF affords isolated solids with no detectable levels of TBA^+ and only minor quantities of F^-, likely present as HF. However, Mo_{24}(5-OH-bdc)$_{24}$ and Mo_{24}(5-Me-phenyloxy-bdc)$_{24}$ materials recovered after TBAX treatment demonstrate retention or a slight decrease in porosity, respectively; Mo_{24}(5-^{t}Bu-bdc)$_{24}$ actually displays an increase in N_2-accessible surface area when precipitating the cage from solutions of both TBACl/DMF and TBAF/DMF with methanol although there is slight variability in the measured surface areas depending on the method and rate of solid isolation.

Isolation of TBAX-treated cages with nonpolar and/or solvents more weakly coordinating than methanol affords a solid with residual-bound halide anion and the necessary charge-balancing TBA cations, as confirmed by ^{1}H NMR and XPS spectroscopy. Although the isolated cages can be resolubilized in DMF or DMSO, they feature significantly decreased surface areas, which is not surprising given the added size and mass of TBAX in their structures. For example, when TBACl-treated Mo_{24}(5-OH-bdc)$_{24}$ is precipitated with Et_2O to afford TBA$_{13}$[Mo_{24}(5-OH-bdc)$_{24}$Cl$_{13}$], the N_2-accessible surface area drops significantly from a BET-(Langmuir) surface area of 647 (726) to 73 (129) m^2/g. Although the presence of coordinated anions and their charge-balancing cations has a deleterious effect on the accessible surface area, the incorporation of charge on otherwise neutral cages opens an exciting avenue for the preparation of porous salts as the majority of permanently microporous cages with high surface area are neutral species.

The most straightforward iteration of this approach involves combining a permanently charged cationic cage with halide-coordinated cage that is otherwise neutral. Given the solution processability, stability, and aversion toward ligand exchange of $Mo_{24}L_{24}$ cages, we prepared a novel cationic cage based on simple ligand functionalization. The reaction of 5-bromomethylisophthalic acid with various amine or imidazole reagents affords ammonium or imidazolium-functionalized cationic ligands, respectively. The reaction of the bromide salt of 5-methylimidazoliumisophthalic acid with $Mo_2(OAc)_4$ affords Mo_{24}(5-MImid-bdc)$_{24}$Br$_{24}$ in nearly quantitative yield. Although this cage is essentially nonporous, it is highly soluble in methanol. Combination of a methanolic solution of Mo_{24}(5-MImid-bdc)$_{24}$Br$_{24}$ and a DMF solution of TBA$_x$[Mo_{24}(5-OH-bdc)$_{24}$Cl$_x$] followed by heating at 85 °C in a N_2 glovebox overnight affords diffraction-quality single crystals of a novel porous salt (Figure 5). Single-crystal X-ray diffraction reveals the two cages are present in a 1:1 ratio as [Mo_{24}(5-OH-bdc)$_{24}$][Mo_{24}(5-MImid-bdc)$_{24}$]X$_{24}$ where X = Cl^- or Br^-. The exact nature and position of the charge-balancing anion could not be determined crystallographically given the inherent disorder in the structure where coordinated solvent, chloride, or bromide can all coordinate to the interior or exterior metal sites of either cage. A distinguishing feature in the crystal structure is the hydroxyl–metal interaction of the 5-hydroxy-isophthalic acid of the Mo_{24}(5-OH-bdc)$_{24}$ cage to the Mo–Mo paddlewheel of the neighboring Mo_{24}(5-MImid-bdc)$_{24}^{24+}$ cage (Figure 5). Consistent with the crystallography, an acid-promoted digestion and ^{1}H NMR of the bulk material confirms the 1:1 ratio of cages in the solid state.

To further confirm the identity of the anions present in the structure, we turned to XPS and EDS. Both methods confirm the presence of chloride in the as-synthesized salt. Importantly,

https://doi.org/10.1021/acs.chemmater.2c01476
Chem. Mater. 2022, 34, 10823–10831

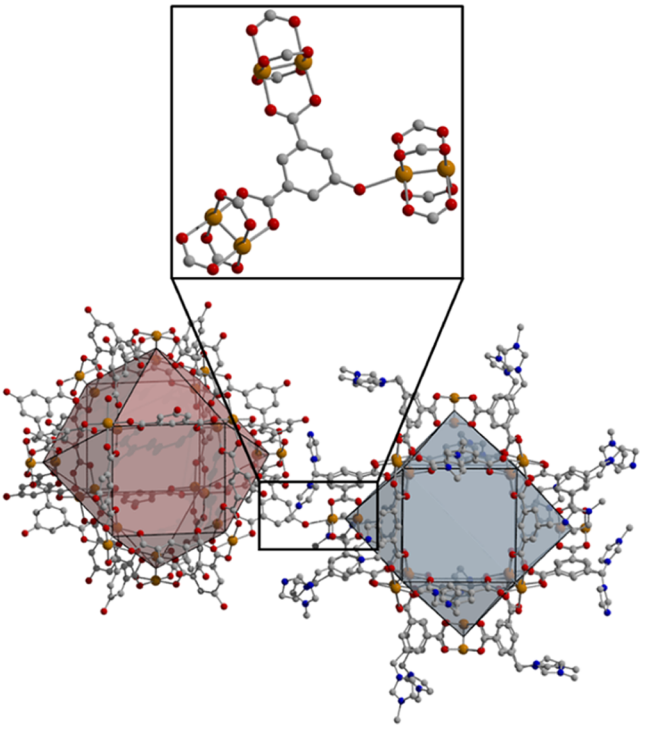

Figure 5. Single-crystal structure of $[Mo_{24}(5\text{-OH-bdc})_{24}][Mo_{24}(5\text{-MImid-bdc})_{24}]Cl_{24}$ where hydroxyl−paddlewheel interactions govern salt formation. Orange, red, blue, and gray spheres represent molybdenum, oxygen, nitrogen, and carbon atoms, respectively. Hydrogen atoms and solvent molecules have been omitted.

XPS and EDS indicate a complete absence of bromide in the structure, while NMR digestions confirm the absence of TBA^+, indicating TBABr is formed as a soluble byproduct of the initial metathesis reaction. Similar to our previously reported porous salts, the product phase is very MOF-like in nature and is completely insoluble in all common organic solvents. Gas adsorption analysis of a suitably washed sample of $[Mo_{24}(5\text{-OH-bdc})_{24}][Mo_{24}(5\text{-MImid-bdc})_{24}]Cl_{24}$ indicates a N_2-accessible surface area of 569 (661) m^2/g, which is only slightly lower than THF-washed $Mo_{24}(5\text{-OH-bdc})_{24}$ and significantly higher than the starting cationic cage, which was essentially nonporous to N_2. Given the strong directional cage−cage interactions in the solid state, the salt displays impressive stability toward solvent evacuation and retains high porosity to activation temperatures as high as 325 °C, which is consistent with thermogravimetric analysis results where $[Mo_{24}(5\text{-OH-bdc})_{24}][Mo_{24}(5\text{-MImid-bdc})_{24}]Cl_{24}$ displays minimal weight loss until decomposition at ∼400 °C. In comparison, while $Mo_{24}(5\text{-OH-bdc})_{24}$ has similar thermal stability and stability toward desolvation, TGA of $Mo_{24}(5\text{-MImid-bdc})_{24}Br_{24}$ indicates gradual decomposition starting at just 250 °C.

Thus far, this novel approach for the synthesis of porous salts has been broadly applicable to various cages of $M_{24}L_{24}$ topology. To assess its generalizability toward additional paddlewheel-based cages, we targeted salts based on M_4L_4 anionic cages and $M_{24}L_{24}$ cationic cages. As the hydroxyl−metal interactions present in $[Mo_{24}(5\text{-OH-bdc})_{24}][Mo_{24}(5\text{-MImid-bdc})_{24}]Cl_{24}$ contributed greatly to the stability and crystallinity of the isolated solid, we prepared an M_4L_4 lantern bearing −OH functional groups on its exterior surface. In a similar manner to the lantern cages discussed above, this poorly soluble cage, $Mo_4(hdp)_4$, can be solubilized via reaction with slight excess of TBAF in DMSO. Although we were unable to obtain diffraction-quality single crystals of this material, methanol diffusion into the DMSO solution of salt afforded $H[Mo_4(hdp)_4F]$ in high yield. The structure contains a fluoride anion between the Mo_2 paddlewheels with a paddlewheel−paddlewheel internal distance of 4.850(1) Å and Mo−F distances of 2.428(2) and 2.552(1) Å. Consistent with the results obtained from crystallographic analysis, digestion and subsequent ^1H NMR spectroscopy confirms the absence of TBA^+ in the initial material.

Introduction of a methanolic solution of $Mo_{24}(5\text{-MImid-bdc})_{24}Br_{24}$ into a DMSO solution of $Mo_4(hdp)_4$ containing a slight excess of TBAF followed by heating at 85 °C in a N_2 glovebox overnight gives a crystalline solid containing both starting cages. Although the crystal structure was not able to be fully resolved due to poor diffraction quality and large amounts of disorder within the structure, the bulk material was determined to have a ∼4:1 ratio of $Mo_4(hdp)_4/Mo_{24}(5\text{-MImid-bdc})_{24}F_{24}$ as confirmed by acid-promoted digestion and subsequent ^1H NMR. Although only portions of the crystal structure were discernible, the cuboctahedral cage is largely fully resolved and the Mo_2−F−Mo_2 units of the lantern are clearly visible. Importantly, the Mo−F−Mo distances within the lantern in the salt are in good agreement with those in $H[Mo_4(hdp)_4F]$ (4.729−4.758 Å vs 4.850(1) Å). The crystallographically determined ratio of cages in the structure suggests a formula of $[Mo_4(hdp)_4]_6[Mo_{24}(5\text{-MImid-bdc})_{24}]F_{24}$, which is in the range of those determined by digestion and ^1H NMR.

While only 6 of the 24 anions in the structure are bound between paddlewheels in the lantern cages, the remaining anions are likely bound to the metal cations of the cationic cage as XPS analysis indicates a single peak at 684.6 eV, which corresponds to metal-bound fluoride in the isolated material. XPS also confirms the absence of bromide as it is removed as TBABr during the course of the metathesis reaction. Finally, EDS spectra show 1.2 wt % of homogeneously distributed fluoride throughout a particle of salt (Figure 6). Appropriately washed and activated $[Mo_4(hdp)_4]_4[Mo_{24}(5\text{-MImid-bdc})_{24}]F_{24}$ displays increased porosity as compared to the parent cages with a N_2-accessible surface area of 212 (271) m^2/g as compared to $Mo_{24}(5\text{-MImid-bdc})_{24}Br_{24}$ with a surface area of 43 (71) m^2/g and $Mo_4(hdp)_4$ with a surface area of 16 (10) m^2/g.

CONCLUSIONS

In this report, we have developed a novel, straightforward post-synthetic method for the solubilization and addition of charge to previously insoluble, neutral cages. We demonstrated that the utilization of TBAX salts can reversibly charge and solubilize both M_4L_4 lanterns and $M_{24}L_{24}$ cuboctahedral cages, with the option of expanding the method to other cage architectures featuring coordinatively unsaturated transition-metal sites. Consequently, this opens up a new library of charged, soluble permanently porous coordination cages that can then be utilized in synthesizing porous salts. As examples of this approach, $Mo_{24}(5\text{-OH-bdc})_{24}$ and $Mo_4(hdp)_4$ were reacted with TBAX salts and combined with positively charged and methanol-soluble $Mo_{24}(5\text{-MImid-bdc})_{24}Br_{24}$ to crystallize salts with concomitant removal of TBABr. The isolated salts, $[Mo_{24}(5\text{-OH-bdc})_{24}][Mo_{24}(5\text{-MImid-bdc})_{24}]Cl_{24}$ and $[Mo_4(hdp)_4]_4[Mo_{24}(5\text{-MImid-bdc})_{24}]F_{24}$, display increased stability toward activation and increased porosity as compared

https://doi.org/10.1021/acs.chemmater.2c01476
Chem. Mater. 2022, 34, 10823−10831

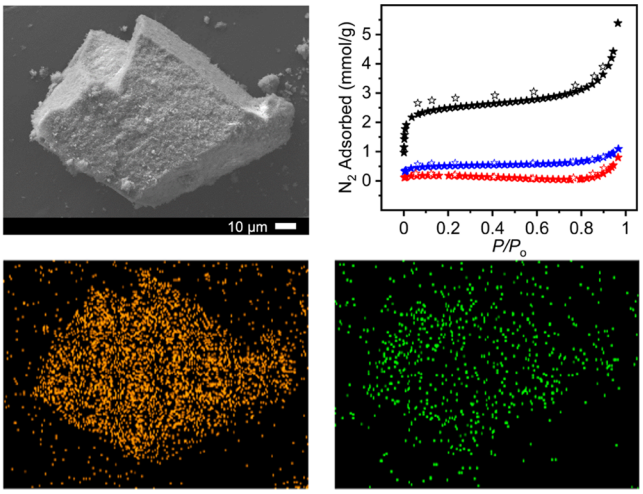

Figure 6. SEM image (top left) and corresponding EDS mapping distribution of a $[Mo_4(hdp)_4]_4[Mo_{24}(5\text{-MImid-bdc})_{24}]F_{24}$ particle. In the EDS maps, orange and green represent Mo (bottom left) and F (bottom right), respectively, showing the homogeneity of fluoride in the bulk material. (Top right) N_2 adsorption in $[Mo_4(hdp)_4]_4[Mo_{24}(5\text{-MImid-bdc})_{24}]F_{24}$ (black) vs parent cages $Mo_4(hdp)_4$ (red) and $Mo_{24}(5\text{-MImid-bdc})_{24}Br_{24}$ (blue) at 77 K. Closed and open symbols denote adsorption and desorption, respectively. The porous salt displays a BET (Langmuir) surface area of 212 (271) m^2/g.

to their parent cages. More importantly, the materials show that this method can be utilized to expand the library of porous salts by including parent porous coordination cages containing building units that afford charge-neutral cages. Going forward, we not only expect that this approach will show tremendous utility in the synthesis of porous salts based on both charged cations and anions but it also can be leveraged for the realization of porous salts where either component is a reactive organometallic fragment rather than a porous ion. Continued advances in this area will open new opportunities in porous, reactive solids.

■ ASSOCIATED CONTENT

Supporting Information

The Supporting Information is available free of charge at https://pubs.acs.org/doi/10.1021/acs.chemmater.2c01476.

Detailed experimental procedures; powder X-ray diffraction data; gas adsorption isotherms; thermal data; and spectroscopic data (PDF)

Structures (CIF)

■ AUTHOR INFORMATION

Corresponding Author

Eric D. Bloch − *Department of Chemistry and Biochemistry, University of Delaware, Newark, Delaware 19716, United States;* orcid.org/0000-0003-4507-6247; Email: edb@udel.edu

Authors

Alexandra M. Antonio − *Department of Chemistry and Biochemistry, University of Delaware, Newark, Delaware 19716, United States*

Michael R. Dworzak − *Department of Chemistry and Biochemistry, University of Delaware, Newark, Delaware 19716, United States*

Kyle J. Korman − *Department of Chemistry and Biochemistry, University of Delaware, Newark, Delaware 19716, United States*

Glenn P. A. Yap − *Department of Chemistry and Biochemistry, University of Delaware, Newark, Delaware 19716, United States;* orcid.org/0000-0003-0385-387X

Complete contact information is available at: https://pubs.acs.org/10.1021/acs.chemmater.2c01476

Notes

The authors declare no competing financial interest.

■ ACKNOWLEDGMENTS

This material is based on work supported by the U.S. Department of Energy's Office of Energy Efficiency and Renewable Energy under the Hydrogen and Fuel Cell Technologies and Vehicle Technologies Offices under Award Number DE-EE0008813. G.P.A.Y. thanks the National Institutes of Health for S10-OD026896A.

■ REFERENCES

(1) Deegan, M. M.; Dworzak, M. R.; Gosselin, A. J.; Korman, K. J.; Bloch, E. D. Gas Storage in Porous Molecular Materials. *Chem. - Eur. J.* **2021**, *27*, 4531−4547.

(2) Lorzing, G. R.; Gosselin, A. J.; Trump, B. A.; York, A. H. P.; Sturluson, A.; Rowland, C. A.; Yap, G. P. A.; Brown, C. M.; Simon, E. D.; Bloch, E. D. Understanding Gas Storage in Cuboctahedral Porous Coordination Cages. *J. Am. Chem. Soc.* **2019**, *141*, 12128−12138.

(3) Liu, X.; Wang, X.; Bavykina, A. V.; Chu, L.; Shan, M.; Sabetghadam, A.; Miro, H.; Kapteijn, F.; Gascon, J. Molecular-Scale Hybrid Membranes Derived from Metal-Organic Polyhedra for Gas Separations. *ACS Appl. Mater. Interfaces* **2018**, *10*, 21381−21389.

(4) Kang, Y.-H.; Liu, X.-D.; Yan, N.; Jiang, Y.; Liu, X.-Q.; Sun, L.-B.; Li, J.-R. Fabrication of Isolated Metal-Organic Polyhedra in Confined Cavities: Adsorbents/Catalysts with Unusual Dispersity and Activity. *J. Am. Chem. Soc.* **2016**, *138*, 6099−6102.

(5) Fang, Y.; Powell, J. A.; Li, E.; Wang, Q.; Perry, Z.; Kirchon, A.; Yang, X.; Xiao, Z.; Zhu, C.; Zhang, L.; Huang, F.; Zhou, H.-C. Catalytic Reactions Within the Cavity of Coordination Cages. *Chem. Soc. Rev.* **2019**, *48*, 4707−4730.

(6) Hosono, N.; Kitagawa, S. Modular Design of Porous Soft Materials via Self-Organization of Metal-Organic Cages. *Acc. Chem. Res.* **2018**, *51*, 2437−2446.

(7) Zhu, W.; Guo, J.; Ju, Y.; Serda, R. E.; Croissant, J. G.; Shang, J.; Coker, E.; Agola, J. O.; Zhong, Q.-Z.; Ping, Y.; Caruso, F.; Brinker, C. J. Modular Metal-Organic Polyhedra Superassembly: From Molecular-Level Design to Targeted Drug Delivery. *Adv. Mater.* **2019**, *31*, No. 1806774.

(8) Dincă, M.; Long, J. R. Introduction: Porous Framework Chemistry. *Chem. Rev.* **2020**, *120*, 8037−8038.

(9) Tian, Y.; Zhu, G. Porous Aromatic Frameworks (PAFs). *Chem. Rev.* **2020**, *120*, 8934−8986.

(10) Geng, K.; He, T.; Liu, R.; Dalapati, S.; Tan, K. T.; Li, Z.; Tao, S.; Gong, Y.; Jiang, Q.; Jiang, D. Covalent Organic Frameworks: Design, Synthesis, and Functions. *Chem. Rev.* **2020**, *120*, 8814−8933.

(11) Slater, A. G.; Little, M. A.; Briggs, M. E.; Jelfs, K. E.; Cooper, A. I. A Solution-Processable Dissymmetric Porous Organic Cage. *Mol. syst. Des. Eng.* **2018**, *3*, 223−227.

(12) Briggs, M. E.; Cooper, A. I. A Perspective on the Synthesis, Purification, and Characterization of Porous Organic Cages. *Chem. Mater.* **2017**, *29*, 149−157.

(13) Taggart, G. A.; Antonio, A. M.; Lorzing, G. R.; Yap, G. P. A.; Bloch, E. D. Tuning the Porosity, Solubility, and Gas Storage Properties of Cuboctahedral Coordination Cages via Amide or Ester Functionalization. *ACS Appl. Mater. Interfaces* **2020**, *12*, 24913−24919.

(14) Rowland, C. A.; Lorzing, G. R.; Gosselin, A. J.; Trump, B. A.; Yap, G. P. A.; Brown, C. M.; Bloch, E. D. Methane Storage in Paddlewheel-Based Porous Coordination Cages. *J. Am. Chem. Soc.* **2018**, *140*, 11153−11157.
(15) Rowland, C. A.; Lorzing, G. R.; Bhattacharjee, R.; Caratzoulas, S.; Yap, G. P. A.; Bloch, E. D. Design and Synthesis of Aryl-Functionalized Carbazole-Based Porous Coordination Cages. *Chem. Commun.* **2020**, *56*, 9352−9355.
(16) Schneider, M. W.; Oppel, I. M.; Griffin, A.; Mastalerz, M. Post-Modification of the Interior of Porous Shape-Persistent Organic Cage Compounds. *Angew. Chem., Int. Ed.* **2013**, *52*, 3611−3615.
(17) Park, J.; Perry, Z.; Chen, Y.-P.; Bae, J.; Zhou, H.-C. Chromium(II) Metal-Organic Polyhedra as Highly Porous Materials. *ACS Appl. Mater. Interfaces* **2017**, *9*, 28064−28068.
(18) Dworzak, M. R.; Deegan, M. M.; Yap, G. P. A.; Bloch, E. D. Synthesis and Characterization of an Isoreticular Family of Calixarene-Capped Porous Coordination Cages. *Inorg. Chem.* **2021**, *60*, 5607−5616.
(19) Carné-Sánchez, A.; Albalad, J.; Grancha, T.; Imaz, I.; Juanhuix, J.; Larpent, P.; Furukawa, S.; Maspoch, D. Postsynthetic Covalent and Coordination Functionalization of Rhodium(II)-Based Metal-Organic Polyhedra. *J. Am. Chem. Soc.* **2019**, *141*, 4094−4102.
(20) Tanabe, K. K.; Cohen, S. A. Postsynthetic Modification of Metal-Organic Frameworks-A Progress Report. *Chem. Soc. Rev.* **2011**, *40*, 498−519.
(21) Gosselin, A. J.; Rowland, C. A.; Bloch, E. D. Permanently Microporous Metal-Organic Polyhedra. *Chem. Rev.* **2020**, *120*, 8987−9014.
(22) Albalad, J.; Carne-Sanchez, A.; Grancha, T.; Hernandez-Lopez, L.; Maspoch, D. Protection Strategies for Directionally-Controlled Synthesis of Previously Inaccessible Metal-Organic Polyhedra (MOPs): The Cases of Carboxylate- and Amino-Functionalized Rh(II)-MOPs. *Chem. Commun.* **2019**, *55*, 12785−12788.
(23) Hernandez-Lopez, L.; Martinez-Esain, J.; Carne-Sanchez, A.; Grancha, T.; Faraudo, J.; Maspoch, D. Steric Hindrance in Metal Coordination Sites Drives the Separation of Pyridine Regioisomers Using Rhodium(II)-Based Metal-Organic Polyhedra. *Angew. Chem., Int. Ed.* **2021**, *60*, 11406−11413.
(24) Grancha, T.; Carne-Sanchez, A.; Hernandez-Lopez, L.; Albalad, J.; Imaz, I.; Juanhuix, J.; Maspoch, D. Phase Transfer of Rhodium(II)-Based Metal-Organic Polyhedra Bearing Coordinatively Bound Cargo Enables Molecular Separation. *J. Am. Chem. Soc.* **2019**, *141*, 18349−18355.
(25) Carné-Sánchez, A.; Craig, G. A.; Larpent, P.; Guillerm, V.; Urayama, K.; Maspoch, D.; Furukawa, S. A Coordinative Solubilizer Method to Fabricate Soft Porous Materials from Insoluble Metal-Organic Polyhedra. *Angew. Chem., Int. Ed.* **2019**, *58*, 6347−6350.
(26) Percástegui, E. G.; Ronson, T. K.; Nitschke, J. R. Design and Applications of Water-Soluble Coordination Cages. *Chem. Rev.* **2020**, *120*, 13480−13544.
(27) Ramsay, W. J.; Ronson, T. K.; Clegg, J. K.; Nitschke, J. R. Bidirectional Regulation of Halide Binding in a Heterometallic Supramolecular Cube. *Angew. Chem., Int. Ed.* **2013**, *52*, 13439−13443.
(28) Custelcean, R. Anion Encapsulation and Dynamics in Self-Assembled Coordination Cages. *Chem. Soc. Rev.* **2014**, *43*, 1813−1824.
(29) Langton, M. J.; Serpell, C. J.; Beer, P. D. Anion Recognition in Water: Recent Advances from a Supramolecular and Macromolecular Perspective. *Angew. Chem., Int. Ed.* **2016**, *55*, 1974−1987.
(30) Rice, C. R.; Slater, C.; Faulkner, R. A.; Allan, R. L. Self-Assembly of an Anion-Binding Cryptand for the Selective Encapsulation, Sequestration, and Precipitation of Phosphate from Aqueous Systems. *Angew. Chem., Int. Ed.* **2018**, *57*, 13071−13075.
(31) Custelcean, R.; Bosano, J.; Bonnesen, P. V.; Kertesz, V.; Hay, B. P. Computer-Aided Design of a Sulfate-Encapsulating Receptor. *Angew. Chem., Int. Ed.* **2009**, *48*, 4025−4029.
(32) Gosselin, A. J.; Decker, G. E.; Antonio, A. M.; Lorzing, G. R.; Yap, G. P. A.; Bloch, E. D. A Charged Coordination Cage Based Porous Salt. *J. Am. Chem. Soc.* **2020**, *142*, 9594−9598.
(33) Gosselin, A. J.; Antonio, A. M.; Korman, K. J.; Deegan, M. M.; Yap, G. P. A.; Bloch, E. D. Elaboration of Porous Salts. *J. Am. Chem. Soc.* **2021**, *143*, 14956−14961.
(34) Ouay, B. L.; Yoshino, H.; Sasaki, K.; Ohtsubo, Y.; Ohtani, R.; Ohba, M. Crystalline Assembly of Metal-Organic Polyhedra Driven by Ionic Interactions with Polyoxometalates. *Chem. Commun.* **2021**, *57*, 5187−5190.
(35) Luo, D.; Zhou, X.-P.; Li, D. Beyond Molecules: Mesoporous Supramolecular Frameworks Self-Assembled from Coordination Cages and Inorganic Anions. *Angew. Chem., Int. Ed.* **2015**, *54*, 6190−6195.
(36) Jackson, N.; Vazquez, I. R.; Chen, Y.-P.; Chen, Y.-S.; Gao, W.-Y. A Porous Supramolecular Ionic Solid. *Chem. Commun.* **2021**, *57*, 7248−7251.
(37) Antonio, A. M.; Korman, K. J.; Deegan, M. M.; Taggart, G. A.; Yap, G. P. A.; Bloch, E. D. Utilization of a Mixed-Ligand Strategy to Tune the Properties of Cuboctahedral Porous Coordination Cages. *Inorg. Chem.* **2022**, *61*, 4609−4617.
(38) *Apex4 [Computer Software]*; Bruker AXS Inc.: Madison, WI, USA, 2021.
(39) Sheldrick, G. M. SHELXT: Integrated space-group and crystal-structure determination. *Acta Crystallogr., Sect. A: Found. Adv.* **2015**, *71*, 3−8.
(40) Sheldrick, G. M. Crystal structure refinement with SHELXL. *Acta Crystallogr., Sect. C: Struct. Chem.* **2015**, *71*, 3−8.
(41) Spek, A. L. Platon Squeeze: a tool for the calculation of the disordered solvent contribution to the calculated structure factors. *Acta Crystallogr., Sect. C: Struct. Chem.* **2015**, *71*, 9−18.
(42) Li, J.-R.; Yu, J.; Lu, W.; Sun, L-B.; Scully, J.; Balbuena, P. B.; Zhou, H.-C. Porous Materials with Pre-Designed Single-Molecule Traps for CO_2 Selective Adsorption. *Nat. Commun.* **2013**, *4*, No. 1538.
(43) Taggart, G. A.; Lorzing, G. R.; Dworzak, M. R.; Yap, G. P. A.; Bloch, E. D. Synthesis and Characterization of Low-Nuclearity Lantern-Type Porous Coordination Cages. *Chem. Commun.* **2020**, *56*, 8924−8927.
(44) Robbins, G. A.; Martin, D. S. Crystal Structures of Tetrakis(μ-formato)dimolybdenum(II)-Potassium Chloride and Two New Polymorphs of Tetrakis(μ-formato)dimolybdenum(II). Single-Crystal Optical Absorption Spectra for Systems with the Molybdenum(II) Formate Dimers. *Inorg. Chem.* **1984**, *23*, 2086−2093.
(45) Sun, H.; DiMagno, S. G. Anhydrous Tetrabutylammonium Fluoride. *J. Am. Chem. Soc.* **2005**, *127*, 2050−2051.
(46) Antonio, A. M.; Korman, K. J.; Yap, G. P. A.; Bloch, E. D. Porous Metal-Organic Alloys Based on Soluble Coordination Cages. *Chem. Sci.* **2020**, *11*, 12540−12546.

https://doi.org/10.1021/acs.chemmater.2c01476
Chem. Mater. 2022, 34, 10823−10831